Magnetic and electric current morphology in the plasma ejected by a laser-irradiated foil

Juan R. Sanmartín
E.T.S.I. Aeronáuticos, Universidad Politécnica, 28040 Madrid, Spain

Peter Reinicke
Max-Planck-Institut für Quantenoptik, 8046 Garching, Germany

(Received 22 February 1990; accepted 19 March 1991)

A quasisteady model for the plasma ablated from a thick foil by a laser pulse, at low $\phi_a \lambda_L^2$ and R/λ_L^2 within a low, narrow range, is given (ϕ_a is absorbed intensity, λ_L wavelength, R focal-spot radius). An approximate analytical solution is given for the two-dimensional plasma dynamics. At large magnetic Reynolds number R_M, the morphology of the magnetic field shows features in agreement with recent results for high intensities. Current lines are open: electric current flows toward the spot near its axis, then turns and flows away. The efficiency of converting light energy into electric energy peaks at $R_M \sim 1$. Both the validity of the model and accuracy of the solution are discussed. The neighborhood of the spot boundary is analyzed in detail by extending classical Prandtl–Meyer results.

I. INTRODUCTION

The coronal plasma ejected by a laser target, if strictly one dimensional, will exhibit neither magnetic field nor electric current. However, two- and three-dimensional geometries do occur in long-pulse, single-beam irradiation of foils and, to a variable extent, in multiple irradiation of pellets. They present, therefore, new or different features with respect to the perfectly plane and spherical cases.

Crossed density and temperature gradients, as an universal cause of large-scale magnetic fields in plasmas, were originally discussed by Biermann.[1] Stamper and Ripin first measured megagauss values in laser plasmas.[2] Time-integrated measurements of magnetic fields, usually performed under unsteady conditions, used magnetic probes, as well as the Faraday and Zeeman effects. For the cylindrically symmetric geometry around a laser beam, the field is dominantly toroidal, though fields along the beam axis have also been found and discussed.[3,4] Reviews have been given by Max[5] and Haines.[6]

In laser fusion the main interest in magnetic effects has been concerned with heat transport. However, full inclusion of its complex algorithm[7,8] in efficient, two-dimensional hydrodynamic codes proves difficult; weakly two-dimensional effects have been considered in the analysis of instabilities and nonuniformities in the corona.[6,9,10] A second point of interest has been the morphology of the magnetic field,[8,11-13] but there is a lack of analytical models that are fully two dimensional and complete.

Here we are concerned with the magnetic morphology, and present one such analytical model for a beam incident on a foil with cylindrical geometry. In the model, neither field nor electric current affect the coronal expansion, which is an isentropic flow (except in a thin layer next to the laser spot on the foil); in particular, heat conduction and absorption by inverse bremsstrahlung are negligible, and ion and electron temperatures, as well as ion and electron mean directed velocities, are nearly equal to each other (local thermodynamic equilibrium). Through Biermann's effect the flow induces a field, subject to both convection and diffusion.

The model is valid for low temperatures and intensities (i.e., low $\phi_a \lambda_L^2$, where λ_L and ϕ_a are laser wavelength and absorbed flux) and R/λ_L^2 within a low, narrow range, R being some appropriate spot radius; this leads to short mean free paths for electrons but not for photons. To be definite, let us say $\phi_a \lambda_L^2 \sim 10^{12}$ W cm^{-2} μm^2 and R/λ_L^2 is around $20\,\mu$m^{-1}. This range is of interest by itself in the broad field of laser interaction with solid matter. In laser fusion, the moderate range $\phi_a \lambda_L^2 \sim 10^{13}$–$10^{14}$ has been of growing interest,[3,14] although most studies have been concerned with higher intensities ($\phi_a \lambda_L^2 \sim 10^{15}$–$10^{17}$).

We here take a foil thick enough so as to neglect its acceleration in the analysis of the corona, and a laser pulse long enough for the coronal flow to be quasisteady ($\tau_L/R \gg 0.01$ nsec/μm for the indicated values of $\phi_a \lambda_L^2$ and R/λ_L^2; τ_L is the pulse half-width). We note that the analyses of both Refs. 12 and 13 were time dependent, retained substantially different ion and electron velocities, and considered $\phi_a \lambda_L^2$ as high as 10^{16} W cm^{-2} μm^2; on the other hand, they ignored the energy equation and field diffusion. In the analytical model of Ref. 12 the electron temperature was taken to be uniform, and only a thin region next to the foil, outside the spot, was considered: some relation between density and magnetic field was needed. In the numerical work of Ref. 13 a specific (constant) temperature profile was chosen.

We introduce the model in Sec. II, and give an approximate solution for the isentropic plasma flow in Sec. III. Both the accuracy of that solution, and the limitations of the model itself are discussed in Sec. IV. We determine magnetic field and electric current in Sec. V, and give a detailed discussion in Sec. VI. An extension of the classical Prandtl–Meyer analysis, for the neighborhood of the spot boundary, is given in the Appendix.

II. BASIC EQUATIONS

In a quasineutral, two-fluid, coronal model that neglects electron inertia and uses classical transport, the equations of

 0899-8221/91/071708-09$02.00

continuity, total momentum, and ion and electron entropies, read[15]

$$\nabla\cdot n\mathbf{v} = 0, \tag{1}$$

$$\tilde{m}n\mathbf{v}\cdot\nabla\mathbf{v} = -\nabla n[T + (T_i/Z_i)] - n\mathbf{u}\wedge(e\mathbf{B}/c), \tag{2}$$

$$\frac{n}{Z_i}T_i\mathbf{v}\cdot\nabla\ln\frac{T_i^{3/2}}{n} = \frac{3m_e n}{Z_i\tilde{m}\tau_e}(T - T_i) \equiv Q_{ei}, \tag{3}$$

$$nT(\mathbf{v}+\mathbf{u})\cdot\nabla\ln\frac{T^{3/2}}{n} = \nabla\cdot\left[nT\left(\frac{\tau_e}{m_e}\gamma\cdot\nabla T - \beta\cdot\mathbf{u}\right)\right] + n\mathbf{u}\cdot\left(\frac{m_e}{\tau_e}\alpha\cdot\mathbf{u} + \beta\cdot\nabla T\right) - Q_{ei} - \nabla\cdot\mathbf{S}_L. \tag{4}$$

Here $Z_i\tilde{m}$, $\mathbf{v}$, and T_i are the ion mass, velocity and temperature; $-e$, m_e, n, $\mathbf{v}+\mathbf{u}$ and T the electron charge, mass, density, velocity and temperature; $\mathbf{B}$ the magnetic field, c the speed of light, $\mathbf{S}_L$ the laser flux, and τ_e a collision time,

$$\tau_e = 3m_e^{1/2}T^{3/2}/4(2\pi)^{1/2}Z_i e^4 n\ln\Lambda,$$

where $\ln\Lambda$ is the Coulomb logarithm. The dimensionless tensors α, β, and γ are of order unity. Their symmetric and antisymmetric parts are even and odd functions of the Hall parameter $\tau_e eB/m_e c$, respectively; they are also functions of the ionization number Z_i.[16]

The model is completed by Ampère's law

$$\nabla\wedge\left(\frac{e\mathbf{B}}{c}\right) = -\left(\frac{2\pi}{\lambda_L}\right)^2\frac{n}{n_c}m_e\mathbf{u} \quad (\nabla\cdot\mathbf{B}=0), \tag{5}$$

where $n_c\propto\lambda_L^{-2}$ is the critical density, and by Faraday's law where the electron momentum equation is used

$$\nabla\wedge\left[\frac{e\mathbf{B}}{c}\wedge(\mathbf{v}+\mathbf{u}) - \left(\frac{m_e}{\tau_e}\alpha\cdot\mathbf{u} + \beta\cdot\nabla T\right)\right] = \nabla T\wedge\nabla\ln n. \tag{6}$$

The equation $\nabla\cdot n\mathbf{u} = 0$ is automatically satisfied.

To simplify the model we make three assumptions:

(i) The mechanical time for a fluid particle to cross a distance equal to some appropriate spot radius R, is small compared with the pulse half-width τ_L,

$$R/v^* \ll \tau_L. \tag{7}$$

The asterisks represent here characteristic values for the corona. We already used condition (7) when dropping $\partial\mathbf{B}/\partial t$ against $\nabla\wedge(\mathbf{v}\wedge\mathbf{B})$ in Faraday's equation, and time derivatives against convective derivatives on the left-hand side of Eqs. (1)–(4) (quasisteady approximation). R is now the characteristic length of the corona.

(ii) The mean free path for absorption of photons by inverse bremsstrahlung is large compared with R,

$$c\tau_e^* \gg R. \tag{8}$$

We may thus neglect the term $\nabla\cdot\mathbf{S}_L$ in Eq. (4).

(iii) The mechanical time is much less than the thermal diffusion time

$$R/v^* \ll m_e R^2/\tau_e^* T_e^*, \tag{9}$$

that is, the first (conductive) term on the right-hand side of (4) is negligible in comparison to its left-hand side, representing convection.

Condition (9) leads to further simplifications. For a quasineutral expansion into vacuum one has $T^*\sim\tilde{m}v^{*2}$. Then (9) is equivalent to $\tau_e^*\tilde{m}/m_e \ll R/v^*$ (thermal equilibration time small compared with the mechanical time); Q_{ei} is thus the dominant term in both (3) and (4), and therefore $T_i\simeq T$. Also, since terms on the left-hand side of (6) can be at most comparable to its right, one gets $u^*/v^*\ll 1$, $\tau_e^* eB^*/m_e c\ll 1$: we can write $\mathbf{v}+\mathbf{u}\simeq\mathbf{v}$, and tensors α, β, γ as functions $\alpha_0,\beta_0,\gamma_0$ of Z_i times the unit tensor so that thermoelectric (β) effects drop off Eqs. (4) and (6). Finally one can show that quadratic terms in $\mathbf{u}$, $\mathbf{B}$ may be dropped from (2), (4) while the α term in (6) must, in principle, be retained.

Equations (1), $T_i = T$,

$$\tilde{m}n\mathbf{v}\cdot\nabla\mathbf{v} = -[(Z_i+1)/Z_i]\nabla(nT), \tag{2'}$$

and the sum of (3) and (4),

$$[(Z_i+1)/Z_i]nT\mathbf{v}\cdot\nabla\ln(T^{3/2}/n) = 0, \tag{10}$$

form a system for density, temperatures, and ion velocity uncoupled from both $\mathbf{u}$ and $\mathbf{B}$, and describe an isentropic flow. Combining (1), (2'), and (10) one obtains the total-energy equation

$$n\mathbf{v}\cdot\nabla\left(\frac{5}{2}\frac{Z_i+1}{Z_i}T + \frac{\tilde{m}v^2}{2}\right) = 0, \tag{11}$$

which can be used instead of (10) or, as in our analysis of the following section, one of the components of the vector equation (2'). Once n, T, and $\mathbf{v}$ have been determined, $\mathbf{B}$ and $\mathbf{u}$ are found from (5) and

$$\nabla\wedge\left(\frac{eB}{c}\wedge\mathbf{v} - \frac{m_e\alpha_0}{\tau_e}\mathbf{u}\right) = \nabla T\wedge\nabla\ln n. \tag{6'}$$

A discussion of the range of validity and accuracy of our model will be deferred to Sec. IV.

III. ISENTROPIC FLOW

To obtain boundary conditions for the plasma dynamics, we note that there must exist a nonisentropic thin layer, next to the target, where both light absorption around the density n_c, and heat conduction taking energy to the ablation surface, are to be retained. Comparing the first and third terms in (4) and using (9) one clearly has

$$\text{layer thickness}\sim\tilde{m}v^*\tau_e^*/m_e \ll R.$$

If the foil is dense and thick enough, the ablation surface may be set at $z=0$ at all times, for the purposes of coronal analysis. The one-dimensional, universal structure of such a layer has been determined in the past. At its exhaust, $z\simeq 0^+$, one finds[17]

$$n_d = \nu(Z_i)n_c, \tag{12a}$$

$$T_d = [Z_i\tilde{m}/(1+Z_i)](3/5)v_d^2, \tag{12b}$$

$$2\nu(Z_i)\tilde{m}n_c v_d^3 = \text{absorbed flux} \equiv \phi_a, \tag{13}$$

where ν varies from 0.61 at $Z_i = 1$ to $\frac{4}{5}$ as $Z_i\to\infty$. For a focal spot with cylindrical geometry, and using cylindrical coordinates r,z,ϕ ($v_\phi = 0$, $\partial/\partial\phi = 0$), the isentropic flow must

start at $z = 0^+$, and within the spot, with the values given by (12) and (13).

We have solved the system (1), (10), (11), and one component of (2'), with the above boundary conditions, in an approximate way. As in all isentropic flows, there are two immediate, exact results; Eqs. (10) and (11) yield

$$T^{3/2}/n = \text{constant along a trajectory}, \tag{14}$$

$$v^2 + 5\frac{Z_i + 1}{Z_i \tilde{m}} T = \text{constant along a trajectory}, \tag{15}$$

which is Bernouilli's equation. We make these results definite by guessing convenient curvilinear, orthogonal coordinates ξ,η in the axial plane: one family of coordinate lines, say $\eta = \text{const}$, is taken as a reasonable approximation to fluid trajectories. This also implies

$$v_\eta = 0. \tag{16}$$

We substitute Eq. (16) for the required equation from (2'), which we now drop entirely.

A good choice is that of oblate ellipsoidal coordinates, defined by

$$(r^2/\xi^2) + z^2/(\xi^2 - 1) = R^2, \quad 1 \leqslant \xi < \infty,$$
$$(r^2/\eta^2) - z^2/(1 - \eta^2) = R^2, \quad 0 \leqslant \eta \leqslant 1,$$

with metric coefficients

$$(\xi^2 - 1)^{1/2} h_\xi = (1 - \eta^2)^{1/2} h_\eta = R(\xi^2 - \eta^2)^{1/2}, \quad h_\phi = R\xi\eta.$$

The axis $r = 0$ corresponds to $\eta = 0$ and arbitrary $\xi \to (1 + z^2/R^2)^{1/2}$. The plane $z = 0$ corresponds to $\xi = 1$ and arbitrary $\eta \to r/R < 1$, or to $\eta = 1$ and arbitrary $\xi \to r/R > 1$. Note that a line of constant η starts perpendicular to the $z = 0$ plane, near it, and ends radially, far away. This is the behavior expected from a trajectory. However, we only have starts for $r < R$, so that our approximation implies a clear-cut boundary for the laser spot. For a given beam profile, one may choose R so as to reduce errors arising from the use of (16).

With the new coordinates, Eq. (1) reads

$$\frac{\partial(h_\eta h_\phi n v_\xi)}{\partial \xi} + \frac{\partial(h_\xi h_\phi n v_\eta)}{\partial \eta} = 0 \tag{17}$$

or, using (16),

$$\left(\frac{\xi^2 - \eta^2}{1 - \eta^2}\right)^{1/2} \xi\eta n v_\xi = \text{function of } \eta.$$

The left-hand sides of (14) and (15), where we now have $v^2 = v_\xi^2$, are only functions of η, too. We finally evaluate all these functions at the point (marked by the value of η considered) where the trajectory leaves the spot:

$$T^{3/2}/n = T_d^{3/2}/n_d,$$
$$v^2 + 5[(Z_i + 1)/Z_i\tilde{m}]T = v_d^2 + 5[(Z_i + 1)/Z_i\tilde{m}]T_d = 4v_d^2,$$
$$(\xi^2 - \eta^2)^{1/2} \xi n v_\xi = (1 - \eta^2)^{1/2} n_d v_d.$$

To write down explicit results, let Φ_{a0} be the absorbed flux at the center of the spot and v_{d0} the corresponding value for v_d, obtained from Eq. (13),

$$v_{d0} = [\Phi_{a0}/2\nu(Z_i)\tilde{m}n_c]^{1/3}. \tag{18}$$

Defining a profile function

$$H \equiv (\Phi_a/\Phi_{a0})^{1/3}, \quad 0 \leqslant r \leqslant R, \tag{19}$$

we arrive at the following solution:

$$v_\xi(s,\zeta) = v_{d0} H(\zeta)[4 - 3y(s,\zeta)]^{1/2}, \tag{20}$$

$$T = [Z_i\tilde{m}/(1 + Z_i)]^{\frac{2}{3}} v_{d0}^2 H^2 y, \tag{21a}$$

$$n = \nu(Z_i) n_c y^{3/2}, \tag{21b}$$

where $y(s,\zeta)$ is given by

$$y^3(4 - 3y) = (1 - \zeta)/s(s - \zeta), \tag{22}$$

varying from $y = 1$ at the spot to $y = 0$ far away. For simplicity of writing we have introduced

$$s \equiv \xi^2, \quad \zeta \equiv \eta^2.$$

Note that $H(0) = 1$, but $H(1) \neq 0$ (in general); values of Φ_a beyond $r = R$ are ignored in our analysis.

IV. ACCURACY AND RANGE OF VALIDITY OF THE SOLUTION

We first can check the accuracy of our approximate results for the plasma dynamics by considering the component of Eq. (2') for v_η,

$$\left(\frac{\xi^2 - 1}{1 - \eta^2}\right)^{1/2} v_\xi \left(\frac{\partial v_\eta}{\partial_\xi} + \frac{\xi v_\eta}{\xi^2 - \eta^2}\right) + v_\eta \frac{\partial v_\eta}{\partial \eta} + \frac{\eta v_\xi^2}{\xi^2 - \eta^2} = -\frac{Z_i + 1}{Z_i \tilde{m}} \frac{1}{n} \frac{\partial}{\partial \eta}(nT).$$

We drop the term quadratic in v_η, which is assumed small, and use the boundary condition $v_\eta = 0$ at $\xi = 1$ to find

$$\frac{v_\eta}{v_\xi} = \left(\frac{\zeta}{4 - 3y} \frac{1 - \zeta}{s - \zeta}\right)^{1/2} \int_1^s \frac{ds'}{2} \left(\frac{s' - \zeta}{s' - 1} \frac{4 - 3y'}{s'}\right)^{1/2} \times \left(\frac{(s' - 1)(1 - y')^{-1}}{4s'y'^2(s' - \zeta)^2} - \frac{1}{s' - \zeta} - \frac{12}{5} \frac{y'}{4 - 3y'} \frac{d \ln H}{d\xi}\right), \tag{23}$$

where $y' \equiv y(s',\zeta)$. This velocity ratio, which should be small, vanishes at $s = 1$, at $\zeta = 0$, and as $s \to \infty$; for a general profile function $H(\zeta)$ the ratio decays as $s^{-1/2}$ at large s. The ratio, on the other hand, shows a weak divergence at $\zeta = 1$, $v_\eta/v_\xi \sim (1 - \zeta)^{-1/6}$. For a special profile, call it $H_*(\zeta)$, we find a faster decay, $v_\eta/v_\xi \sim s^{-2/3}$. The definition of $H_*(\zeta)$ requires that the integral in (23) vanishes as $s \to \infty$ $(0 < \zeta < 1)$. This profile, however, is unphysical: $dH_*/d\xi$ is positive for $\zeta > 0.843...$ and H_* itself diverges as $\zeta \to 1$. There is also a special, though again unphysical, type of profile function, $H \sim (1 - \zeta)^{-5/3}$, for which we have $v_\eta/v_\xi \sim (1 - \zeta)^{1/2}$ as $\zeta \to 1$.

Consider now a Gaussian beam profile, $\Phi_a/\Phi_{a0} = \exp(-r^2/r_f^2)$ with given r_f. Choosing $R = 6^{1/2} r_f$ and $3^{1/2} r_f$ we have $H = e^{-2\zeta}$ and $e^{-\zeta}$, respectively. Figure 1 shows v_η/v_ξ for (a) $H = e^{-2\zeta}$ and (b) $H = e^{-\zeta}$. Also shown is the case (c) $H = H_*(\zeta)$ if $\zeta < 0.843...$, $H = H_*(0.843...)$ otherwise [for ζ below and not very close

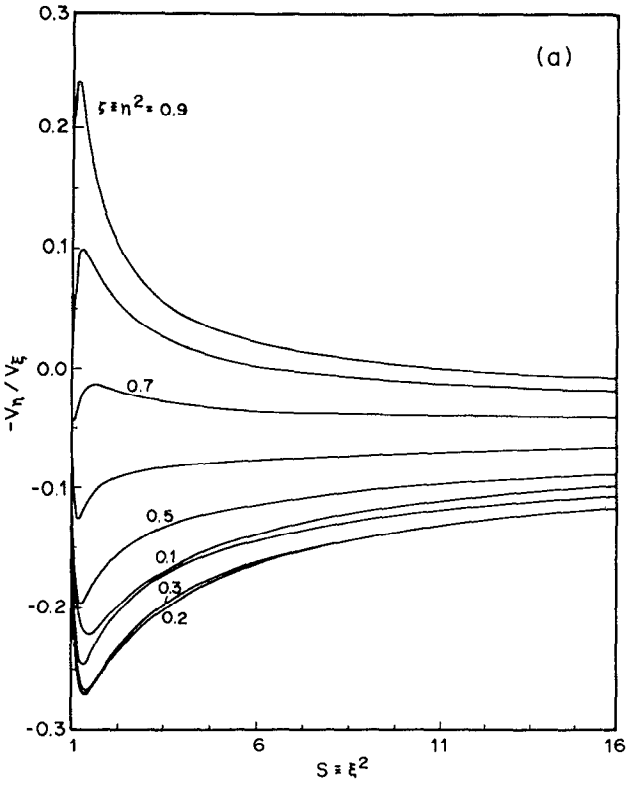

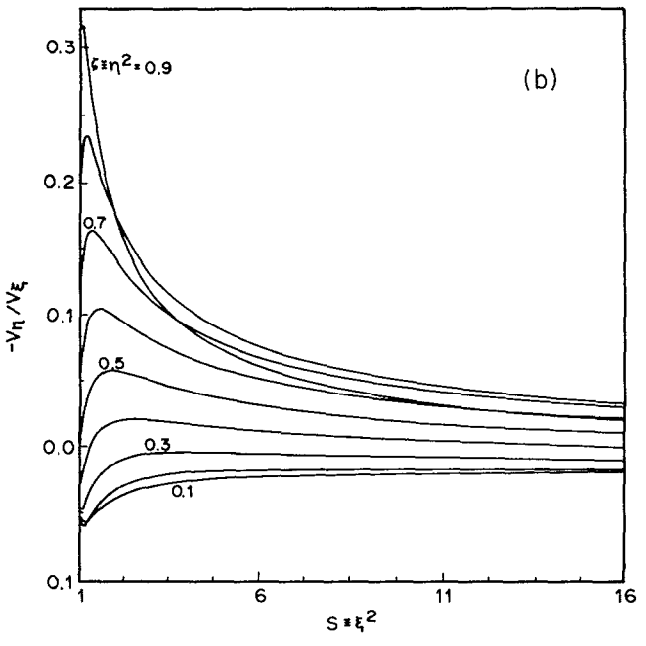

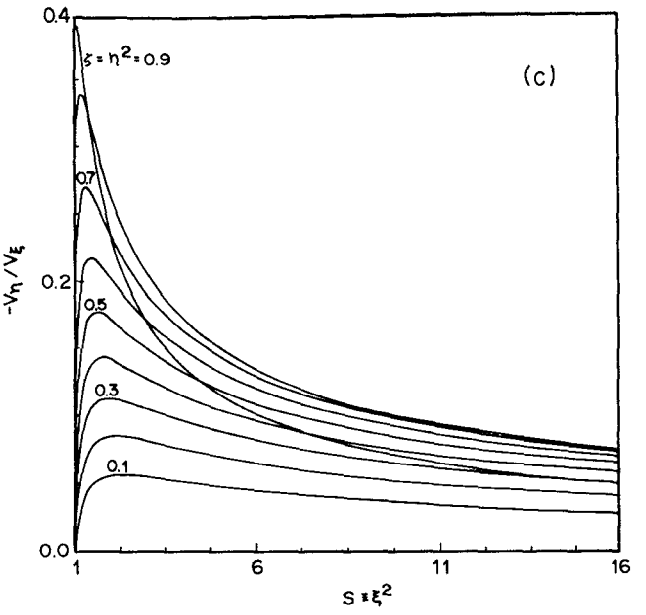

FIG. 1. Velocity ratio v_η/v_ξ versus ellipsoidal coordinates ξ, η for a Gaussian radial distribution of absorbed flux Φ_a, truncated at $r = R$: (a) $\Phi/\Phi_{\infty 0} = \exp(-2r^2/R^2)$; (b) $\Phi_a/\Phi_{\infty 0} = \exp(-r^2/R^2)$; (c) $\Phi_a/\Phi_{\infty 0} \simeq \exp(-0.45r^2/R^2)$ for $r < 0.92R$, constant thereafter.

to 0.843... one has $H_*(\zeta) \simeq \exp(-0.45\zeta)$]. Clearly $R = 3^{1/2} r_f$ is the best choice; Fig. 1(b) shows that its velocity ratio is indeed small except for ζ close to unity and, simultaneously, s in some neighborhood of unity, that is, near the boundary of the spot as expected. Note that the errors in evaluating the right-hand sides of Eqs. (14) and (15), and dropping the second term of (17), are of first order in v_η/v_ξ, while the error in writing v_ξ^2 for v^2 is second order. For trajectories leaving the spot at $r < 0.77R$ ($\zeta \equiv \eta^2 < 0.59$), $|v_\eta/v_\xi|$ is everywhere less than 0.1. For the trajectory with $r \simeq 0.87R$ at the spot, v_η/v_ξ has a maximum of 0.2, but lies below 0.1 beyond $z \simeq 0.84R$, $r \simeq 1.69R$. The neighborhood of the spot boundary is analyzed as a Prandtl–Meyer expansion in the Appendix.

Figures 2 and 3 show lines of constant density and temperature, respectively, in the axial plane; for Fig. 3, and further results in the following section, we took $H = e^{-\zeta}$. A nonvanishing right-hand side in (6) arises from having vari-

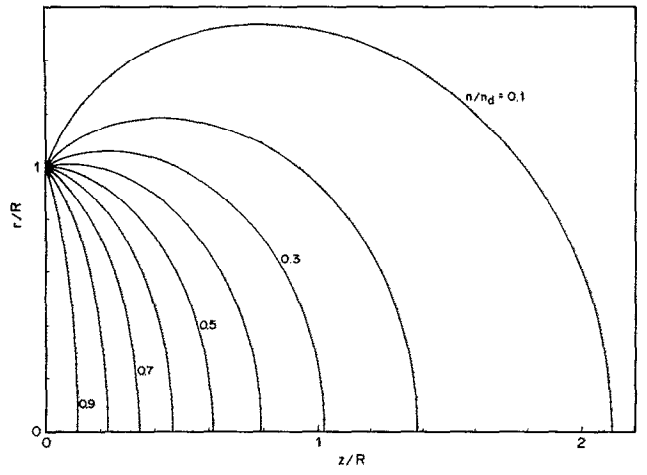

FIG. 2. Isodensity lines in the axial plane; n_d is density at the exhaust of the conduction layer.

able temperature T_d but constant density n_d on the spot. Note the behavior far from the spot, $(r^2+z^2)n \simeq \frac{1}{2}R^2 n_d \times \cos(\text{angle of radius vector with } z \text{ axis})$.

We now check the consistency of our model, as given in Sec. II. Condition (8) requires negligible absorption within the isentropic region, during both the inward and outward ray trajectory. For a ray incident along the z axis, that means $2\int_0^\infty k_a dz \ll 1$, where $k_a = n/n_c c\tau_e(1-n/n_c)^{1/2}$ is the absorption coefficient for inverse bremsstrahlung; a straightforward calculation yields

$$R/\tau_{d0} \ll [1.18/\nu(Z_i)]c. \tag{8'}$$

Condition (9) requires a heat-flux divergence, $\nabla\cdot(nT\tau_e\gamma_0 m_e^{-1}\nabla T)$, small compared with, say, the first term on the left-hand side of (11). At a point on the z axis that means

$$f\left(\frac{z}{R}\right)\frac{\gamma_0(Z_i)Z_i A_i^{1/2}}{(1+Z_i)^{3/2}}\left(\frac{T_{d0}}{m_e}\right)^{1/2} \ll \frac{R}{\tau_{d0}}, \tag{9'}$$

where A_i is the atomic number and $f=0$, 2.6, and 8.9 for $z\to\infty$, $z=2R$ and $z=0$, respectively. Condition (9') is easier to satisfy at lower Z_i and A_i/Z_i.

From (8') and (9') we derive an upper bound for T_{d0}. For a CH_2 target and coronal ions H^+ and C^{4+}, we have mean values $\langle A_i\rangle = 14/3$, $\langle Z_i\rangle = 2$ ($\nu \simeq 0.66$); at $z=2R$, we then obtain

$$T_{d0} \ll 15.1 \text{ keV}.$$

The range for R, defined by both (8') and (9'), comes out to be very narrow: Take $T_{d0}=0.2$ keV (corresponding to $\Phi_{a0}\lambda_L^2 = 1.70\times10^{12}\,\mathrm{W\,cm^{-2}}\,\mu\mathrm{m}^2$) and $\lambda_L = 1.06\,\mu$m; using $\ln\Lambda \simeq 4.8$, $\langle Z_i^2\rangle/\langle Z_i\rangle = 3$, one finally has $\tau_{d0} \simeq 1.04\times10^{-13}$ sec and

$$6.5\ \mu\text{m} \ll R \ll 61\ \mu\text{m}.$$

Thus conditions (8') and (9') can be satisfied barely simultaneously and the accuracy is about 30%. Note that for R at the lower (higher) end of its range, heat conduction (inverse bremsstrahlung) should have some effect throughout the corona. Since energetics is not the prime consideration here, and on grounds of simplicity, one might then consider using a polytropic law, $\mathbf{v}\cdot\nabla(T/n^{\alpha-1})=0$ instead of the adiabatic or isentropic law given by Eq. (10), for which $\alpha = \frac{5}{3}$.[18] Results quite similar to those in Sec. III would follow.

We note finally that for laser and coronal parameters as considered above, and $R\sim 20\,\mu$m, condition (7) requires a pulse half-width τ_L about or longer than 10^{-9} sec.

V. ELECTRIC CURRENT AND MAGNETIC FIELD

We now determine **B** and **u** from Eqs. (5) and (6'), taking the results for fluid variables n, T, and v_ξ from Sec. III. Note that τ_e, being only a function of entropy, is independent of s: $\tau_e = \tau_d(\xi) \equiv \tau_{d0}H^3$. Eliminating **u**, the induction equation for the magnetic field, which is toroidal, reads

$$\frac{\partial}{\partial s}\left[\left(\frac{s-1}{\xi(1-\xi)}\right)^{1/2}\frac{H^{-3}}{y^{3/2}}\frac{\partial}{\partial s}(s^{1/2}b)\right] + \frac{\partial}{\partial\xi}\left[\left(\frac{1-\xi}{s(s-1)}\right)^{1/2}\frac{H^{-3}}{y^{3/2}}\frac{\partial}{\partial\xi}(\xi^{1/2}b)\right] = R_M H\frac{\partial}{\partial s}\left[\frac{18}{5}y\frac{dH}{d\xi} + \left(\frac{s-\xi}{\xi(1-\xi)}\right)^{1/2}(4-3y)^{1/2}b\right], \tag{24}$$

where

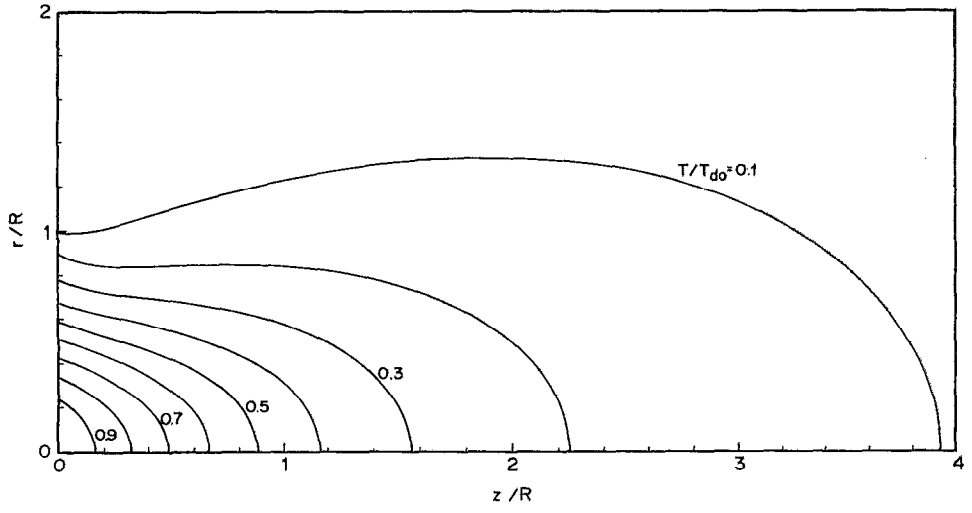

FIG. 3. Isotemperature lines in the axial plane, for the case of Fig. 1(b); T_{d0} is exhaust temperature at the center of the spot.

$$b \equiv \frac{1+Z_i}{Z_i \tilde{m}} \frac{eRB_\phi}{c v_{d0}}, \quad R_M \equiv \frac{2\pi^2 \nu(Z_i) v_{d0} \tau_{d0} R}{\alpha_0(Z_i) \lambda_L^2},$$

R_M being a magnetic Reynolds number. With $b(s,\zeta,R_M)$ being known, Eq. (5) gives U,

$$U_\xi = \frac{-1}{y^{3/2}} \left(\frac{1-\zeta}{s-\zeta}\right)^{1/2} \frac{\partial}{\partial \zeta}(\zeta^{1/2} b), \tag{25}$$

$$U_\eta = \frac{1}{y^{3/2}} \left(\frac{s-1}{s-\zeta}\right)^{1/2} \frac{\partial}{\partial s}(s^{1/2} b), \tag{26}$$

where

$$\mathbf{U} \equiv \frac{2\pi^2 R^2}{\lambda_L^2} \frac{m_e}{\tilde{m}} \frac{1+Z_i}{Z_i} \nu(Z_i) \frac{\mathbf{u}}{v_{d0}}.$$

Boundary conditions for Eq. (24) can be obtained from an examination of the appropriate current-density component at each boundary. At $\zeta = 0$ we have $nu_\eta = 0$ by symmetry. By requiring a bounded u_η we have $nu_\eta \to 0$ as $\zeta \to 1$: There is no target charging outside the spot. Similarly, by requiring a bounded u_ξ we have $nu_\xi \to 0$ (more strongly, $s^{1/2} nu_\xi \to 0$) as $s \to \infty$. Finally, and as it comes out from the structure of the conduction layer, there is no local charging of the target within the spot: $nu_\xi = 0$ at $s = 1$ for all ζ.

From Eq. (25) we next have $\zeta^{1/2} b = \text{const}$ at $s = 1$ and as $s \to \infty$. Also, from Eq. (26), we have $s^{1/2} b = \text{const}$ at both $\zeta = 0$ and $\zeta = 1$. Then, by requiring a bounded b at the center of the spot, one easily arrives at a general condition

$$b = 0,$$

throughout the entire contour. Equation (24) is now a linear, nonhomogeneous, elliptic equation with Dirichlet boundary conditions. There exists a unique solution $b(s,\zeta,R_M)$ for each value of R_M and each profile function $H(\zeta)$.

Particularly simple is the limit case $R_M \to \infty$, for which convection of the magnetic field dominates its diffusion. We find

$$b = \frac{18}{5}(1-y) \left(\frac{\zeta(1-\zeta)}{(s-\zeta)(4-3y)}\right)^{1/2} \frac{dH}{d\zeta}. \tag{27}$$

Figure 4 shows constant b lines in the axial plane for $H = e^{-\zeta}$. Note that the field decays slowly as distance to the spot increases ($b \sim s^{-1/2}$) and that the distance of peak field to target, at given r, increases with r. For $\langle Z_i \rangle = 2$, $\langle A_i \rangle = 14/3$, $T_{d0} = 0.2\,\text{keV}$, $\lambda_L = 1.06\,\mu\text{m}$, and $R = 20\,\mu\text{m}$, we have $R_M \simeq 8.0$, $B_{\max} \simeq 4.0 \times 10^5$ G.

There is a subset of constant b lines in Fig. 4 reaching the spot boundary so that the field presents a maximum in between vanishing values, inside and outside the spot. This large R_M behavior is *not*, however, a result of our using the approximate solution of Sec. III; actually, that behavior disappears when the diffusive, or resistive, term in the induction equation, which becomes dominant close enough to the point $z = 0$, $r = R$, is retained (see the Appendix). Thus, the magnetic field is, in fact, well defined and vanishing at that point, constant b lines turning around without reaching it.

Explicit expressions for the components of U can be obtained from (25) and (26); Figures 5 and 6 show these components. For a given ζ there is at most one value of s such that U_ξ vanishes (U_ξ takes a finite value at infinity). It follows that current lines are open. In fact, at large s we find

$$U_\xi \propto \frac{d}{d\zeta}\left(\zeta(1-\zeta)^{1/2} \frac{dH}{d\zeta}\right);$$

for $H = e^{-\zeta}$, one has $U_\xi \gtrless 0$ for $\zeta \lessgtr \frac{1}{2}$: at angles $\tan^{-1}(r/z) < 45°$ electron velocity exceeds ion velocity, for $\tan^{-1}(r/z) > 45°$ ion velocity is larger. Current flows from infinity

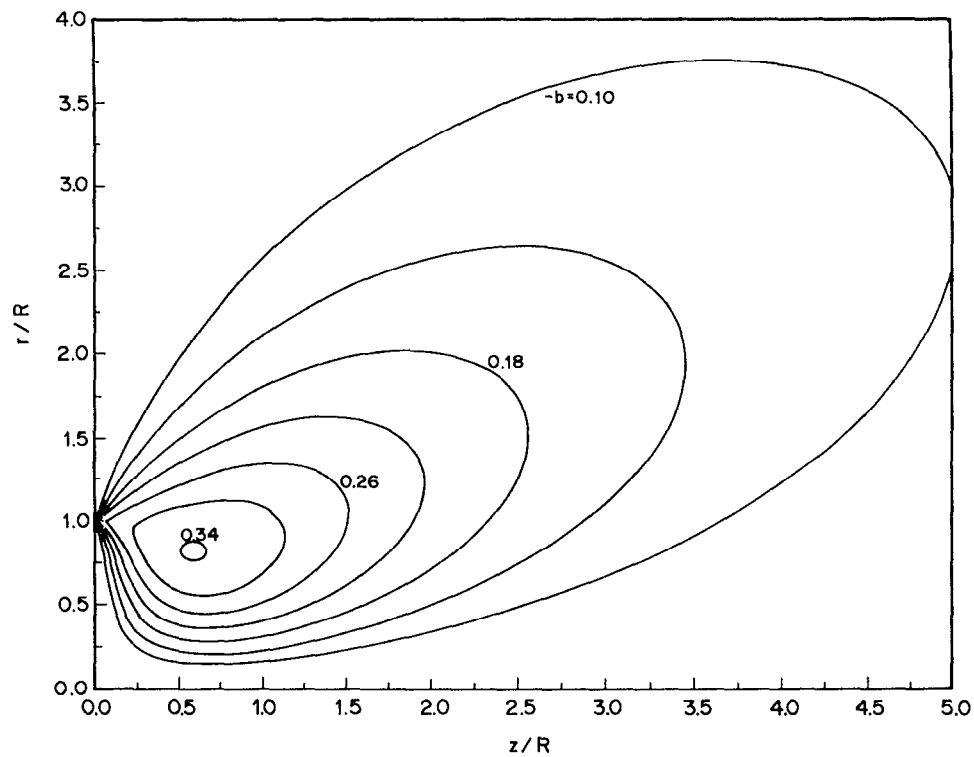

FIG. 4. Contour plot of (azimuthal) normalized magnetic field for the case of Fig. 1(b), at large magnetic Reynolds R_M; within a thin, resistive neighborhood of the spot boundary, results are invalid.

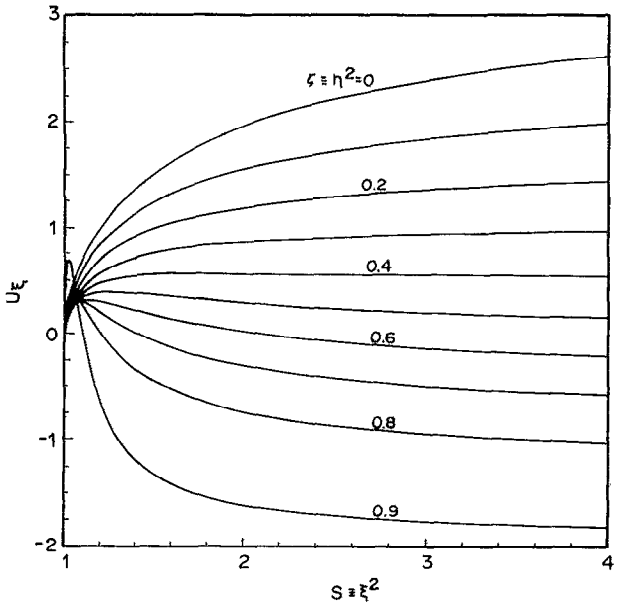

FIG. 5. Component along ellipsoidal coordinate ξ of normalized, electron velocity relative to ions for the case of Fig. 1(b), at large R_M.

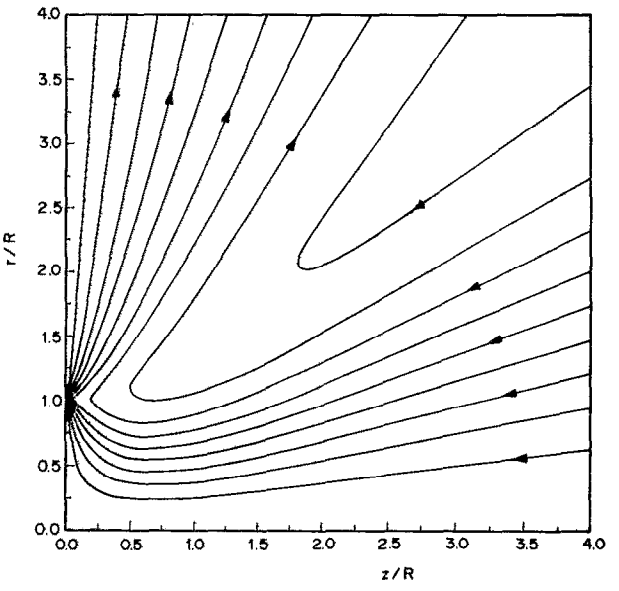

FIG. 7. Current-flow lines for the case of Fig. 1(b), at large R_M; the resistive neighborhood of spot boundary is as in Fig. 4.

toward the target near the z axis, it flows outward closer to the target. Charge cups, used to determine ion spectra,[12] could pick up the current in an experimental test.

Figure 7 for current-flow lines in the axial plane, shows the spot boundary acting as both a charge source and sink (of equal strength: it collects no net current). Again, however, this is not a consequence of approximation (16) in Sec. III, stemming, instead, from our neglect of the small resistive region around the singular point. The Appendix shows that within this region current lines turn smoothly to return to infinity: no line reaches the spot boundary.

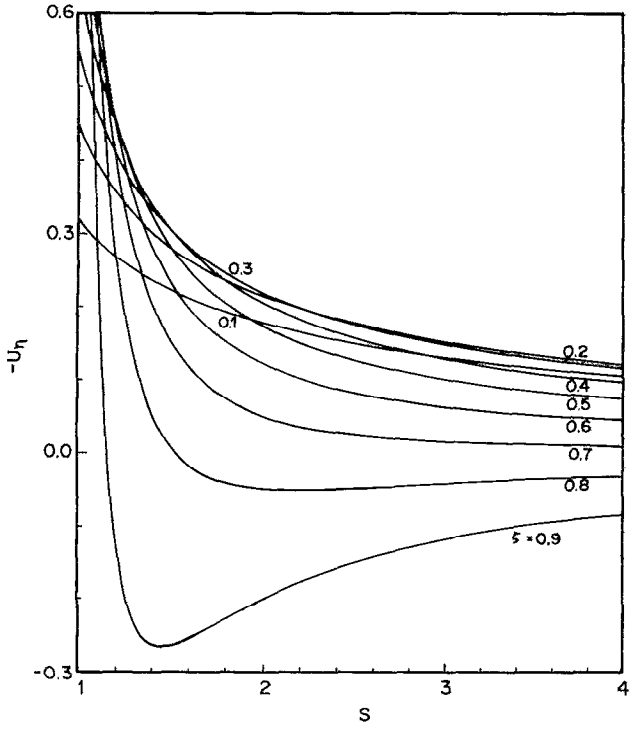

FIG. 6. Same as in Fig. 5 for the component along ellipsoidal coordinate η.

The total current coming from infinity is, for $H = \exp(-\zeta)$,

$$I = e(2\pi)\int_0^{2^{-1/2}} d\eta \lim_{\xi\to\infty}(h_\eta h_\phi n u_\xi)$$
$$= \frac{9\exp(-\frac{1}{2})}{20(2^{1/2})}\frac{Z_i\tilde{m}c^2}{(1+Z_i)e^2}ev_{d0},$$

basically dependent on flow velocity v_{d0}. In our regime (Sec. II), the electron momentum equation, at large R_M, reads

$$0 = -\nabla(nT) - en(\mathbf{E}+\mathbf{v}\wedge\mathbf{B}/c) - \beta_0 n\nabla T,$$

from which Eq. (6′), without the diffusion term, is obtained. Far from the target, where $\mathbf{E}\simeq -\mathbf{v}\wedge\mathbf{B}/c$, the potential drop from $\zeta = 0$ to $\zeta = \frac{1}{2}$ is

$$V = \int_0^{2^{-1/2}} d\eta \frac{h_\eta v_\xi B}{c} = -\frac{\frac{3}{2}[1-\exp(-1)]T_{d0}}{e}.$$

For $Z_i = 2$, $A_i = 14/3$, and $T_{d0} = 0.2$ keV, one obtains $I = 4.6$ kA, $V \simeq -190$ V.

As in ionospheric-satellite applications,[19] the induced field $-\mathbf{v}\wedge\mathbf{B}/c$ would put energy into any electric load connecting charge collectors; kinetic energy would be extracted from the flow through the braking magnetic force $-en\mathbf{u}\wedge\mathbf{B}/c$. Here both **u** *and* **B** would be modified by the connection; they would remain, however, of the same order as found in our solution if the load impedance is or order V/I as determined above. The power conversion ratio,

$$\frac{\text{generated electric power}}{\text{absorbed light power}} \sim \frac{VI}{\pi R^2\phi_{a0}} = \frac{6.1Z_iA_i^{1/2}}{\alpha_0(1+Z_i)^{3/2}}\frac{\tau_{d0}}{R}\left(\frac{T_{d0}}{m_e}\right)^{1/2}\frac{1}{R_M}, \quad (28)$$

would be small, according to conditions (9′) and $R_M \gg 1$.

One easily finds that for $R_M \ll 1$ it suffices to change $1/R_M \to R_M$ for (28) to hold. Thus, the power ratio peaks at $R_M \sim 1$, the maximum being still small according to (9′). This is, of course, as expected, because in our regime, magnetic and current effects could be neglected in the determination of n, T, and $\mathbf{v}$ [and in the energy equation (11)], the flow being approximated as isentropic.

Note that, according to (28), if condition (9′) breaks down, and conduction becomes dominant throughout the corona, the power ratio should be some fraction of order unity.

VI. DISCUSSION

We have considered the generation of magnetic field $\mathbf{B}$, and current density $-en\mathbf{u}$, in the plasma ejected by a laser-irradiated foil, assuming that the flow is quasisteady, inverse bremsstrahlung negligible, and heat conduction restricted to a thin layer next to the spot, where absorption around critical density n_c occurs. Outside that layer (which provides the boundary conditions), the flow is then isentropic and affected by neither $\mathbf{B}$ nor $\mathbf{u}$. We obtain an approximate analytical solution to the two-dimensional plasma dynamics. The solution involves a free parameter, "spot radius" R, that can be adjusted for each laser beam profile so as to reduce errors in the approximation. Detailed results for the case of a Gaussian beam are shown to be quite accurate, except near the spot boundary.

The nonuniform entropy at the layer exhaust (due to a nonuniform light intensity across the beam) gives rise, through the usual $\nabla T \wedge \nabla \ln n$ term in the induction equation, to a toroidal magnetic field. A unique solution is proved to exist for arbitrary magnetic Reynolds number R_M. In the limit $R_M \to \infty$ (when field convection dominates diffusion) the solution is given explicitly. The far field is found to decrease as the inverse distance from the spot; and its peak at given r lies farther from the target at larger r. These same features have been noticed, for quite different conditions, in experimental[11] numerical,[8] and analytical studies.[12]

Ampère's equation yields a (poloidal) current in the axial plane. For $R_M \to \infty$ current lines are open: The radial component of $\mathbf{u}$ does not vanish at infinity. Current is found to flow from infinity, toward the spot, at solid angles near the beam axis, and flow away at angles closer to the foil. The conversion ratio for collection of the faraway current (electric power/absorbed light power) peaks at $R_M \sim 1$. Although the maximum ratio is small in the regime here considered, it increases to a value of order unity when conduction is dominant throughout the expanding plasma.

An exact (Prandtl–Meyer) analysis of the neighborhood of the spot boundary, including induction and Ampère equations, is given in the Appendix; it shows that no matter how large R_M is, there is a resistive region, of thickness R/R_M, where diffusion is dominant. Current lines, and lines of constant B, are pressed together in this thin region around the spot boundary.

The simultaneous neglect of inverse bremsstrahlung and heat conduction in the large isentropic region requires, roughly,

$$(T/m_e)^{1/2} \ll R/\tau_e \ll c,$$

where τ_e and T are characteristic electron collision time and temperature. Reasonably low temperatures lead to a narrow range of allowed values for the quantity R/λ_L^2; for $\lambda_L = 1.06\,\mu$m, very small spots ($R \simeq 20\,\mu$m) are required. Targets with low atomic mass and ionization number are favored. Typically the quasisteady assumption implies pulses over 10^{-9} sec long. At large R_M and temperatures of a few hundred eV, currents in excess of 1 kA are obtained. Qualitatively our results remain valid if weak, instead of strong, inequalities are used in the conditions above.

ACKNOWLEDGMENTS

We acknowledge helpful criticism by the referee.

This work was supported in part by D. G. Investigación Científica y Técnica, Spain, and Kernforchungszentrum Karlsruhe G.M.B.H., Germany (A.I.20); and in part (J.R.S.) by the Comisioń Interministerial de Ciencia y Technología of Spain (PB87 0569).

APPENDIX: APPROXIMATE VERSUS EXACT SOLUTION NEAR THE SPOT BOUNDARY

The analysis of the region around the spot boundary $z = 0$, $r = R$, requires using polar coordinates ρ, θ centered at this singular point. We have

$$z = \rho \sin\theta, \quad r = R - \rho\cos\theta,$$

θ varying from zero at the target surface within the spot ($r < R$) to π again at the surface, outside the spot ($r > R$). As $\rho/R \to 0$ we have both $s \to 1$ and $\zeta \to 1$, leading to

$$\begin{aligned} &\rho/R \simeq (1-\zeta)/2 + (s-1)/2, \\ &\theta \simeq 2\tan^{-1}[(s-1)/(1-\zeta)]^{1/2}, \\ &[0 \leqslant (s-1)/(1-\zeta) < \infty]. \end{aligned} \tag{A1}$$

We now consider the behavior of the approximate results of Secs. III and V within this small region, and compare them with locally exact results, here obtained.

(i) Equations (20), (21), and (23) take the form

$$T/T_{d1} = (n/n_d)^{2/3} = y, \quad v_\xi/v_{d1} = (4-3y)^{1/2},$$

$$\frac{v_\eta}{v_\xi} = \frac{3}{2} y^{3/2} \int_y^1 \frac{dy'\, y'^{-3}(1+y')(1-3y'^2)}{(4-3y')^{1/2}(3y'^2+2y'+1)^{1/2}},$$

where $v_{d1} = v_{d0}H(1)$ (v_{d0}/e for $H = e^{-\xi}$). For $y(\theta)$ we get, from (22) and (A1),

$$y^3(4-3y) \simeq (1-\zeta)/(s-\zeta) \to \cos^2(\theta/2) \quad [0 \leqslant y(\theta) \leqslant 1]. \tag{A2}$$

Note that this solution, being independent of ρ, is of the similarity type. For $y \to 0$ ($\theta \to \pi$), we find $v_\eta/v_\xi \simeq 1/2y^{1/2} \sim (1-\zeta)^{-1/6}$, as it had been found, in general, for $\zeta \to 1$ (Sec. IV).

Exact results can be found by observing that, as $\rho \to 0$, one can drop $\partial/\partial\rho$ terms (against $\rho^{-1}\partial/\partial\theta$ terms) everywhere in Eqs. (1), (2′), and (10). This leads to the well-known (Prandtl–Meyer) isentropic, expansion flow around a corner:[20]

$$T/T_{d1} = (n/n_{d1})^{2/3} = \cos^2(\theta/2),$$

$$v_\theta/v_{d1} = \cos(\theta/2), \quad v\rho/v_{d1} = 2\sin(\theta/2).$$

Having a specific-heat ratio of $\frac{5}{3}$ like a monatomic gas, the plasma that leaves the target with $v_\rho = 0$ at $r < R$ $(\theta = 0)$ turns 90° to flow along the target surface at $r > R$ $(\theta = \pi)$ with vanishing v_θ, n, and T. We can easily obtain, from v_ρ and v_θ above,

$$\frac{v_\xi}{v_{d1}} = \frac{3 - \cos\theta}{2}, \quad \frac{-v_\eta}{v_\xi} = \frac{\sin\theta}{3 - \cos\theta}.$$

Note that this exact solution is also independent of ρ. It agrees with our approximate results for T, n, and v_ξ above at both $\theta = 0$ and $\theta = \pi$. In between the agreement is reasonable: At $\theta = \pi/2$, for instance, the exact values for T and v_ξ are 18% lower and 2% higher, respectively. More important, the exact result for the ratio $-v_\eta/v_\xi$ is bounded for all θ: It has a maximum, $1/2^{3/2} \simeq 0.354$, at $\theta \simeq 70.5°$. This bound, though not too small, reinforces the discussion of Sec. III on the validity of our approximate solution, outside the small ρ/r region.

(ii) The large R_M results of Sec. V were based on our solution in Sec. III. For $s \to 1$, $\zeta \to 1$, $H = e^{-\zeta}$, we obtain, using (A2),

$$-b = (18/5e)(1 - y)y^{3/2}.$$

Also, from U_ξ and U_η, we easily obtain

$$\frac{U_\theta}{U_\rho} \to 0, \quad U_\rho = \frac{R}{\rho}\frac{3}{8e}(4 - 3y)^{1/2}(3y^2 + 2y + 1)^{1/2}\frac{y - \frac{3}{5}}{y^{3/2}}.$$

Thus, both b and ρU_ρ are again functions of θ only. Note that, while b vanishes at both $\theta = 0$ and π, its value at the spot boundary, being a function of θ, depends on how the limit $\rho \to 0$ is approached; $-b$ has a maximum, 0.246, at $y = \frac{3}{5}$ $(\theta \simeq 92.8°)$. At this angle U_ρ vanishes and is positive (negative) at smaller (larger) angles. All this is in agreement with Figs. 4 and 7. The radial current density $(\sim -y^{3/2}U_\rho)$ diverges like $1/\rho$ as ρ vanishes, so that the singular point collects a finite current within the range $0 < \theta < 92.8°$, and ejects the same current within the range $92.8° < \theta < \pi$.

Exact results for **B** can be found from the induction equation by using the approach, and formulas, for the Prandtl–Meyer expansion. At large R_M we have $\nabla \wedge [(e\mathbf{B}/c) \wedge \mathbf{v}] = \nabla s \wedge \nabla T$, where $s \equiv$ entropy $= \ln(T^{3/2}/n)$; in polar coordinates,

$$\frac{eB}{c}v_\rho + \frac{\partial}{\partial\theta}\frac{eB}{c}v_\theta = \frac{\partial T}{\partial\theta}\frac{\partial s}{\partial\rho}.$$

Note that the $\partial s/\partial\rho$ term, being the product of two derivatives, remains dominant as $\rho \to 0$; we dropped, however, a term $-(\partial T/\partial\rho)(\partial s/\partial\theta)$: Equation (8) shows that entropy, as opposite to other variables, has comparable derivatives along ρ and θ. From the formulas for v_ρ, v_θ we can obtain the equation for the trajectories, $\rho\cos^4\theta/2 = \rho(\theta = 0) \equiv \rho_0$, along which the entropy is constant [Eq. (10)]. At $\theta = 0$ we have $s = \ln(T_{d0}^{3/2}/n_d) + 3\ln H$; since $\zeta = (1 - \rho_0/R)^2$ we obtain, for $H = e^{-\zeta}$, $s \simeq \text{const} + 6\rho_0/R$. Hence,

$$\frac{\partial s}{\partial\rho} = 6R^{-1}\cos^4\theta/2,$$

and, thus, the induction equation yields

$$-b = (9/5e)(1 - \cos\theta)\cos^3(\theta/2).$$

From Ampère's law one then obtains

$$\frac{U_\theta}{U_\rho} \to 0, \quad U_\rho = \frac{R}{\rho}\frac{9}{10e}\sin\theta\left(1 - \tfrac{3}{2}\tan^2\frac{\theta}{2}\right).$$

These exact results show the same features of our approximate solution; the maximum of $-b$ (0.246 again) occurs at $\theta \simeq 78.5°$, where ρU_ρ vanishes.

The above comparisons prove that the peculiar behavior of Figs. 4 and 7 at the spot boundary is not due to approximation (16) of Sec. III. In fact, the behavior is due to our ignoring a resistive boundary layer that must surround that point, at large magnetic Reynolds numbers. At $\rho \sim R/R_M \ll R$, one finds that the diffusion term must be retained in the induction equation; for $\rho \ll R/R_M$ that term alone is dominant, leading to

$$\frac{\partial(n^{-2/3}\partial b/\partial\theta)}{\partial\theta} = 0.$$

From conditions $b = 0$ at $\theta = 0, \pi$, one gets $b = 0$ at all θ. U_ρ does not, now, diverge as $\rho \to 0$, and neither constant b lines, nor current lines, reach the boundary spot.

[1] L. Biermann, Z. Naturforsch. A **5**, 65 (1950).
[2] J. A. Stamper and B. H. Ripin, Phys. Rev. Lett. **34**, 138 (1975).
[3] J. Briand, J. C. Kieffer, A. Gomes, C. Arnas, J. P. Dinguirard, Y. Quemener, L. Berge, M. El Tamer, and M. Armengaud, Phys. Fluids **30**, 2893 (1987).
[4] B. Chakraborty, M. Khan, B. Bhattacharyya, S. Deb, and H. C. Pant, Phys. Fluids **31**, 1303 (1988); R. Dragila, *ibid.* **30**, 925 (1987).
[5] C. E. Max, in *Laser Plasma Interaction*, Proceedings of Les Houches Summer School on Theoretical Physics 1980, edited by R. Balian and J. C. Adam (North-Holland, Amsterdam, 1982), p. 301.
[6] M. G. Haines, Can. J. Phys. **64**, 912 (1986).
[7] R. J. Mason and C. W. Cranfill, IEEE Trans. Plasma Sci. **PS-14**, 45 (1986).
[8] J. M. Wallace, J. U. Brackbill, and D. W. Forslund, J. Comput. Phys. **63**, 434 (1986).
[9] D. A. Tidman, Phys. Fluids **18**, 1454 (1975).
[10] J. R. Sanmartín, J. Sanz, and J. A. Nicolás, Phys. Lett. A **124**, 81 (1987); J. Sanz, J. A. Nicolás, J. R. Sanmartín, and J. Hilario, Phys. Fluids **31**, 2320 (1988).
[11] M. D. J. Burgess, B. Luther-Davies, and K. A. Nugent, Phys. Fluids **28**, 2286 (1985).
[12] S. R. Goldman and R. F. Schmalz, Phys. Fluids **30**, 3608 (1987).
[13] T. J. M. Boyd and D. Cooke, Phys. Fluids **31**, 651 (1988).
[14] O. Willi, C. Duncan, and P. T. Rumsby, Opt. Commun. **37**, 40 (1981).
[15] J. R. Sanmartín, Laser Part. Beams **7**, 219 (1989).
[16] S. I. Braginskii, in *Reviews of Plasma Physics*, edited by M. A. Leontovich (Consultants Bureau, New York, 1965), Vol. 1, p. 205.
[17] J. R. Sanmartín and A. Barrero, Phys. Fluids **21**, 1957 (1978).
[18] E. N. Parker, *Interplanetary Dynamical Processes* (Wiley, New York, 1963), Chaps. 4–7.
[19] M. Martínez-Sanchez and D. E. Hastings, J. Astron. Sci. **35**, 75 (1987).
[20] L. D. Landau and E. M. Lifshitz, *Fluid Mechanics* (Pergamon, Oxford, 1966), Secs. 101 and 104.